Biomacromolecules

Article

pubs.acs.org/Biomac

Identification of Wet-Spinning and Post-Spin Stretching Methods Amenable to Recombinant Spider Aciniform Silk

Nathan Weatherbee-Martin,[†] Lingling Xu,[†] Andre Hupe,[∥] Laurent Kreplak,[‡] Douglas S. Fudge,[∥] Xiang-Qin Liu,[†] and Jan K. Rainey*[,†,§]

[†]Department of Biochemistry & Molecular Biology; [‡]Department of Physics & Atmospheric Science and School of Biomedical Engineering; [§]Department of Chemistry, Dalhousie University, Halifax, Nova Scotia B3H 4R2, Canada

[∥]Department of Integrative Biology, University of Guelph, Guelph, Ontario N1G 2W1, Canada

ABSTRACT: Spider silks are outstanding biomaterials with mechanical properties that outperform synthetic materials. Of the six fibrillar spider silks, aciniform (or wrapping) silk is the toughest through a unique combination of strength and extensibility. In this study, a wet-spinning method for recombinant *Argiope trifasciata* aciniform spidroin (AcSp1) is introduced. Recombinant AcSp1 comprising three 200 amino acid repeat units was solubilized in a 1,1,1,3,3,3-hexafluoro-2-propanol (HFIP)/water mixture, forming a viscous α-helix-enriched spinning dope, and wet-spun into an ethanol/water coagulation bath allowing continuous fiber production. Post-spin stretching of the resulting wet-spun fibers in water significantly improved fiber strength, enriched β-sheet conformation without complete α-helix depletion, and enhanced birefringence. These methods allow reproducible aciniform silk fiber formation, albeit with lower extensibility than native silk, requiring conditions and methods distinct from those previously reported for other silk proteins. This provides an essential starting point for tailoring wet-spinning of aciniform silk to achieve desired properties.

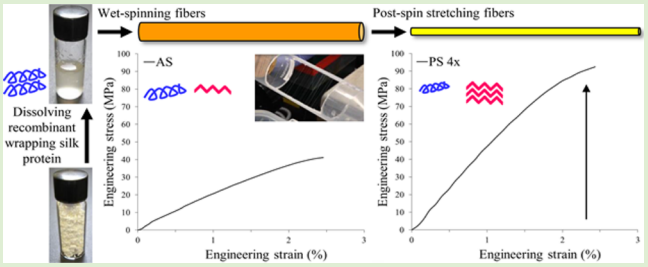

INTRODUCTION

Spider silks are extraordinary biomaterials with diverse and impressive mechanical properties. A combination of high tensile strength and extensibility make them mechanically superior to synthetic materials such as Kevlar and nylon.[1] This, along with their excellent bioresponse properties in vivo, makes them highly sought after for industrial and biomedical applications.[2−5]

Spiders produce up to seven types of silk, protein-based materials serving different biological functions such as web construction and locomotion (major ampullate (MA), or dragline, silk), prey capture (flagelliform silk), egg casing (tubuliform silk), or wrapping of prey (aciniform silk).[5] Unlike with silkworms, harvest of large amounts of silk from spiders is infeasible due in part to territorial and cannibalistic behavior.[6] This is further confounded by the fact that mechanical properties of spider silks vary due to a variety of factors dependent upon spider condition, including nutrition and environment, making harvest of consistent material a challenge.[7] To date, artificial spider silk production has met with limited success and it has been argued that this is due to a lack of identification of appropriate, biomimetic spinning conditions.[8] Artificial spider silk production has been most successful for MA silk,[9−16] the best understood class of spider silk.

Native aciniform silk protein (spidroin), AcSp1, from *Argiope trifasciata* consists of a core domain with at least 14 consecutive 200 amino acid repeat units (referred to as "W" units herein) with identical primary structure that comprise >95% of the protein sequence.[17] MA spidroin also contains a core repetitive domain, but its primary structure is dramatically different with a 25−40 amino acid domain of Ala_n motifs spaced by Gly-rich repeats that is reiterated up to ∼100 times.[18−20] The Ala- and Gly-rich domains are associated with tensile strength and extensibility, respectively.[21] AcSp1 is distinct from MA spidroin, as it does not contain short motifs. Rather, although it is rich in Ser, Ala, and Gly, it is relatively heterogeneous through the 200 amino acid domain and has a wide amino acid composition.[17]

Aside from the core repetitive domain, AcSp1 has flanking short, nonrepetitive N- and C-terminal domains[22] as with MA spidroins.[23,24] Although it is known that the nonrepetitive terminal domains play roles in solubilization and polymerization of the spidroins, they do not appear to directly modulate the resulting mechanical properties of MA silk fibers.[25] Instead, it is the central repetitive core domain within the spidroin tripartite structure that is correlated with and influences mechanical properties.[25−27]

Secondary structure composition is also distinct between MA and AcSp1 spidroins. In solution, MA spidroins exhibit ∼30% α-helix, 30% β-turn, and 40% random coil with a complete loss of α-helical character and transformation during fibrillogenesis to a state containing 36−37% β-sheet oriented parallel to the

Received: June 10, 2016
Revised: July 5, 2016
Published: July 7, 2016

DOI: 10.1021/acs.biomac.6b00857
Biomacromolecules 2016, 17, 2737−2746

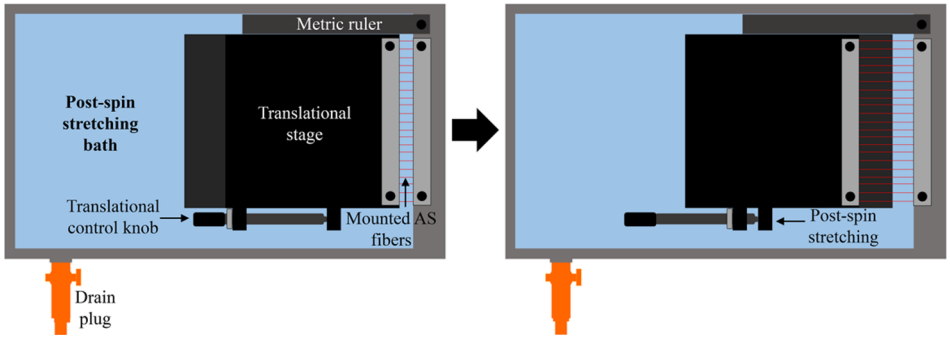

Figure 1. Schematic of the post-spin stretching apparatus for W_3 fibers. The translational control knob allows for controlled motion of the stage, the metric ruler allows for consistent and precise measurement of fiber stretching, and the drain plug allows bath drainage at a controlled rate.

fiber long axis and surrounded by amorphous regions.[28−31] AcSp1 undergoes a conceptually similar structural transition, but this results in a highly distinct fibrous structuring. In solution, AcSp1 from *A. trifasciata* is composed of compactly structured ∼138 residue globular helical/turn containing domains connected together by 62 residue intrinsically disordered linkers.[32] Upon fiber formation, the protein retains a similar proportion of disorder and turn content alongside a mixture of moderately oriented β-sheet (∼30%) and α-helical (∼24%) domains.[33,34]

Corresponding to its distinctive primary and secondary/tertiary structuring, the strength, extensibility, and toughness of aciniform silk also differ significantly from other types of spider silk. Most notably, native aciniform silk exhibits the greatest toughness of the silks.[17,22] As with the MA spidroins, the conformational transformation from α-helix to β-sheet is believed to be a key component in providing strength to silk fibers.[35] The role of the distinctive oriented helices is less clear but seems likely to contribute to aciniform silk's unique extensibility. As a whole, the direct link between structure and function remains elusive in aciniform silk particularly given the lack of short motifs traditionally associated with strength or extensibility.

We have previously expressed recombinant AcSp1-derived constructs with varying numbers of W units (nomenclature: W_n, n = number of repeats) in *Escherichia coli*[36] and demonstrated that W_2, W_3, and W_4 constructs can be hand-pulled from low-concentration buffered aqueous solutions to form multi-centimeter fibers.[32,36] However, low-concentration solutions are inefficient for high-yield fiber production and we have found that increasing W_n concentration in aqueous solution promotes nonproductive aggregation (results not shown).

A number of methods have been utilized to spin spider silks from dope solutions including electrospinning,[37−40] microfluidics,[41] and wet-spinning.[9−12,14,15,42−45] Because wet-spinning has been extensively employed on recombinant spidroins, alongside recombinant honeybee silk,[46] and regenerated *Bombyx mori* silkworm fibroin,[47−50] we focused on applying this technique to AcSp1. In wet-spinning, a spinning dope is subjected to shear force followed by extrusion into a coagulation bath, serving to amalgamate the protein in a solid fiber. This is often coupled to a post-spin stretching step, which is carried out by stretching wet-spun fibers in a solvent to promote structural changes within the fiber leading to corresponding changes in mechanical properties such as strength, extensibility, and toughness.[9,12,15,43,49,51−53]

Here we report a wet-spinning method using the W_3 AcSp1 construct as a starting point for reproducible high-throughput aciniform silk fiber formation. Despite the wide variety of recombinant silk wet-spinning methods noted above, previously reported conditions and methods were not amenable to W_3. Each step in the process required distinct adaptation during development of a wet-spinning protocol suitable for AcSp1. Although the resulting fiber properties are not native-like through this wet-spinning method, primarily due to lower extensibility, the capability to wet-spin AcSp1 is key for downstream technological applications. Furthermore, identification of wet-spinning conditions suitable for AcSp1 is essential for subsequent process optimization.

MATERIALS AND METHODS

Solubilization of W_3 Protein. Lyophilized W_3 was prepared as previously described.[36] Spinning dopes were made by suspending ∼8% (w/v) lyophilized W_3 protein powder into 70% 1,1,1,3,3,3-hexafluoro-2-propanol (HFIP)/30% H_2O (v/v) in glass vials. HFIP (≥99.0% (GC); grade: puriss; Sigma-Aldrich, Oakville, ON) and H_2O was type I distilled. Suspensions were vortexed until homogeneous and sonicated twice (37 °C, 5 min) with vortexing in between. Subsequently, the glass vials were wrapped with aluminum foil to prevent exposure of the suspensions to light and incubated for ∼48 h at room temperature with occasional vortexing. After 48 h, the suspensions were centrifuged (18 000 rcf, 30 min, 20 °C) and transferred into new glass vials. This was repeated until the suspensions (now spinning dopes) were transparent with no visible insoluble components remaining.

Protein concentration in each spinning dope was estimated for aliquots at a 1/100 dilution based on absorbance (A) at 214 nm (8452A UV/vis spectrophotometer, Hewlett-Packard, Palo Alto, CA) using a quartz cuvette with a path length of 0.05 cm (Hellma, Mülheim, Germany). The Beer−Lambert law could then be used to estimate concentration, $c = A/\varepsilon l$, where l is the path length of the cuvette (in cm) and ε is the extinction coefficient (in $L{\cdot}mol^{-1}{\cdot}cm^{-1}$ at 214 nm), calculated for W_3 to be 816 334 $L{\cdot}mol^{-1}{\cdot}cm^{-1}$ based on the quantitative relationships detailed by Kuipers and Gruppen.[54] If the estimated concentration was lower than ∼8% (w/v), evaporation was allowed to take place until a final concentration of ∼8% (w/v) was reached.

Viscosities for neat 70% HFIP/30% H_2O and for a variety of W_3 solutions (employing an N-terminally His-tagged protein) were measured in triplicate at 22.5 °C using a microviscometer (*micro*Visc HVROC-L, RheoSense, San Ramon, CA). Reading error is reported on the basis of instrumental accuracy (2% of reading).

Wet-Spinning To Form As-Spun (AS) Fibers. Spinning dope was loaded into a 100 μL Hamilton reversible needle (RN) syringe (Hamilton, Reno NV), which was attached to 6 cm long polyetheretherketone (PEEK) tube (outer diameter, 1/16 in.; inner diameter, 0.005 in.; Sigma-Aldrich) by RN compression fittings (1/16

DOI: 10.1021/acs.biomac.6b00857
Biomacromolecules 2016, 17, 2737−2746

in.; Hamilton). The syringe containing the spinning dope was securely attached to a syringe pump (KD Scientific KDS100, Holliston, MA) and the dope was extruded through the PEEK tube into a coagulation bath of 95% ethanol (EtOH)/5% dH_2O at a constant speed of 16 μL/min. Fibers formed in the coagulation bath were carefully picked up using tweezers and guided onto a 50 mL conical centrifuge tube (Fisher Scientific; Ottawa, ON) as a collector. This was attached to a rotator (LKB 2232 MicroPerpeX S Pump; GE Healthcare Life Sciences, Mississauga, ON) set to spin at a constant speed equivalent to the extrusion rate.

Post-Spin Stretching of AS Fibers. A custom-designed apparatus was built (Department of Physics & Atmospheric Science Machine Shop, Dalhousie University, Halifax, NS) to allow for consistent and controlled stretching of fibers in dH_2O (Figure 1; materials: container, aluminum; metric ruler and bolt, stainless steel; single axis translation stage (50 mm, Thor Laboratories, Montreal, QC), anodized aluminum). AS fiber samples were macroscopically examined for defects before a post-spin stretching treatment. AS fiber pieces 2-3 cm in length without visible defects were cut and placed at the edge and on top of the translational stage and at the edge and on top of the container mounting surface using Scotch Double Sided Tape (1/2 in., 3M Canada, London, ON). Scotch Magic Tape (3/4 in., 3M Canada) was then carefully placed on top to firmly secure both ends of the AS fibers. Following fiber affixing, the post-spin stretching apparatus was slowly filled with dH_2O until the fibers were fully immersed. Using the control knob, the fibers were smoothly stretched to 2× or 4× their original length and allowed to rest in the dH_2O bath for 3 min. The dH_2O bath was then drained, while simultaneously misting the surface with 95% EtOH to prevent tension between the water−fiber interface, until fibers were no longer in contact with dH_2O. Subsequently, the resulting "post-spun (PS)-stretched" fibers were allowed to dry at room temperature for 5−10 min.

Light Microscopy. AS and PS fibers were placed on a glass slide (Fisher Scientific; Ottawa, ON) and fiber morphology was observed by imaging with a 10× or 40× objective lens coupled with a 10× ocular lens, using an Axiovert 200 M inverted optical microscope coupled to an AttoArc2 HBO 100W lamp (Carl Zeiss Canada, Toronto, ON). Images were acquired with a ORCA-R2 digital camera (Hamamatsu Corporation, Bridgewater, NJ).

Far-UV Circular Dichroism (CD) Spectroscopy. CD spectra of neat spinning dopes and 1/10 dilutions were recorded using a J-810 spectropolarimeter (Jasco, Easton, MD). All measurements were carried out at room temperature using a quartz cuvette with 0.001 cm path length (Hellma, Mülheim, Germany). A sensitivity of 100 mdeg was employed and data were collected from 260 to 180 nm at 50 nm/min with 0.1 nm data pitch. At least three repetitions (including blanks) were performed for each sample. Spectra were averaged, blank subtracted, and converted to mean residue ellipticity on the basis of concentration determined by absorbance at 214 nm (as detailed above).

Fiber Diameter Determination. Fibers were cut into 2 cm long pieces and mounted on 3 × 2 cm rectangular testing cards with a 1 cm gap in the middle for mechanical testing. Prior to mechanical tests, mounted fibers were examined by optical microscopy and discarded if there were any apparent defects, such as uneven thickness or damage. Utilizing an inverted optical microscope with a 10× ocular lens and a 10× objective lens (Axio Observer A1, Carl Zeiss Canada), three micrographs were taken along the long axis of each fiber, one near the middle and two near each end of the fiber. Using ImageJ 1.48v (National Institutes of Health, Bethesda, MD), fiber diameters were measured (based on a calibration standard with 10 μm spacing) at 6 different positions for each micrograph; fiber diameters were derived from the average of these 18 measurements. The Poisson ratio (ν)[55] for a given stretched fiber was calculated as

$$\nu = -\frac{\varepsilon_y}{\varepsilon_x} \tag{1}$$

where ε_x and ε_y are the axial and lateral strains, respectively, given by

$$\varepsilon_x = \frac{L - L_0}{L_0} \tag{2}$$

and

$$\varepsilon_y = \frac{D - D_0}{D_0} \tag{3}$$

based upon the length (L_0) and diameter (D_0) before stretching and those after stretching (L and D, respectively).

Mechanical Testing. Mechanical testing was performed at room temperature and 32 ± 4% humidity using a Nano Bionix instrument (MTS Nano Instruments, Eden Prairie, MN) with a 10 mm gauge length, an extension rate of 0.1 mm/s, and a tension trigger of 10 μN. Data were transferred to the instrument software (MTS Testwork 4.09A) and exported to Microsoft Excel 2013. Engineering strain was calculated as the change in length divided by the original length and engineering stress was calculated as the force divided by the fiber's resting cross-sectional area (based on fiber diameter.) Extensibility and strength were taken as the measured strain and stress at failure, respectively. Data were plotted as stress−strain curves, allowing both Young's modulus and toughness to be calculated. Young's modulus was determined as the slope of the initial linear portion (using the range of 0.3−1.5% engineering strain to avoid nonlinearity at the extrema) of the stress−strain curve and toughness was calculated as the area under a given stress−strain curve. Microsoft Excel 2013 was used to conduct statistical tests, employing a two-tailed t-test to test for a significant ($P < 0.001$) difference in tensile strength between AS and PS 4× W_3 fibers.

Polarized Light Microscopy. Fibers were visualized using an Eclipse 600 microscope (Nikon Canada Inc., Mississauga, ON) equipped with cross-polarizing filters and a quarter wave plate analyzer allowing passage of elliptically polarized light. A 10× ocular lens was used with a 40× objective lens to detect birefringence. Images were captured using an AmScope 10MP Microscope Digital Camera (Irvine, CA) and a Nikon TV lens C-0.45x.

Raman Spectromicroscopy. A diffraction limited Raman scattering setup was modified from Gullekson et al.[56] and consisted of an inverted microscope (1X71; Olympus, Center Valley, PA) coupled with an iHR550 Raman Spectrometer (Horiba Jobin Yvon, Edison, NJ). Spectra were recorded at room temperature at 35 ± 5% humidity using a 532 nm line (far-field) solid-state laser (Ventus Vis, Laser Quantum, Cheshire, UK) for excitation, and focused using a 60× objective lens to a diameter of approximately 1 μm. The exposure power was ∼0.5 mW with an optical density of 0.4 and a confocal pinhole diameter of 200 μm. After passage through an edge filter, scattered light was collected over a spectral range of 400−1800 cm^{-1} and resolved using the Raman spectrometer. For a given condition, average values from 3−4 independent fibers were obtained at 3−4 different positions along the long axis of the fiber at either 0° or 90° (manual 90° rotation) fiber alignment relative to the incident polarized light. Fibers were routinely checked optically for structural deterioration from the laser, but no apparent damage occurred under these conditions.

Spectral manipulation and analysis were carried out with the software GRAMS/AI 9.0 (Thermo Scientific, Markham, ON). Peak correction was performed to eliminate any background fluorescence or cosmic spike interference that may have generated artifacts within the spectra. This was followed by baseline correction with a cubic function and 7-point spectral smoothing. A total average was then taken for each fiber condition for both the perpendicular and parallel alignment positions relative to the incident polarized scattered light. The conformation-sensitive spectra were then plotted for comparison purposes between the two alignment positions for any given fiber condition. It should be noted that some degree of displacement could not be avoided during manual rotation of the samples. Orientation-independent spectra could not be acquired with this instrument, so quantification of β-sheet and α-helical content was not carried out. However, decomposition of the amide I region using Gaussian fitting, as described previously,[31,57] was carried out for qualitative comparison purposes. The peak fitting of the amide I region was carried out in the

DOI: 10.1021/acs.biomac.6b00857
Biomacromolecules 2016, 17, 2737−2746

manner described by Rousseau and colleagues[57] for each alignment. The boundaries for the bandwidth positions at ~1670 and ~1657 cm^{-1} were ≤18.0 cm^{-1}, whereas for all other amide I components and side chain components they were ≤20.0 cm^{-1}. The center points for each band were restrained to only be moved by ±1.0 cm^{-1}.

Scanning Electron Microscopy (SEM). The SEM imaging protocol was adapted from that which we employed previously.[36] Briefly, fibers for cross-sectional imaging were initially prepared as described above for diameter determination and mechanical testing but were mounted on a testing card with a 1 mm gap instead of a 1 cm gap. Each mounted fiber was then immersed in liquid nitrogen for at least 15 s, followed by folding of both ends of the card to break the fiber in the gap region. For each condition, testing cards with fractured fiber ends were fixed on an SEM stub at an angle of ~45°. Once fixed, fibers were coated with Au/Pd particles using a low vacuum coater (EM ACE200, Leica Microsystems Inc., Richmond Hill, ON) prior to acquiring SEM micrographs in secondary electron collection mode using a S-4700 Cold Field Emission SEM (Hitachi, Toronto, ON).

Atomic Force Microscopy (AFM). Fibers for AFM imaging were carefully placed on a glass slide (Fisher Scientific, Ottawa, ON) coated with a thin film of fresh LePage Epoxy glue (Henkel Canada Corporation, Mississauga, ON). Samples were allowed to sit at room temperature for at least 60 min to allow the epoxy to cure. AFM images were acquired using a NanoWizard II Ultra (JPK, Berlin, Germany) mounted on an inverted optical microscope (Axio Observer A1, Carl Zeiss Canada) operating in intermittent-contact mode (room temperature, at 24 ± 2% relative humidity) with silicon cantilevers having a nominal resonance frequency of ~300 kHz and force constant of 40 N/m (Tap 300-G, Budget Sensors, Sofia, Bulgaria). AFM micrographs were then processed with v3.3.32 NanoWizard IP software (JPK) and exported as TIFF files.

RESULTS AND DISCUSSION

Production and Characterization of W_3 Protein Dope.

The first distinctive aspect of AcSp1 behavior is apparent in spinning dope production. To date, 100% HFIP has been used to dissolve recombinant MA,[9−13,42,51,58] recombinant flagelliform,[11,42] and recombinant cylindriform/tubuliform[43,59] spidroins. Beyond the use of 100% HFIP, a number of protocols have employed denaturing conditions[14,15] or, in one instance, phosphate buffered saline[45] to dissolve recombinant MA-based spidroins. The W_3 protein could not be dissolved in 100% HFIP. Through screening of a variety of HFIP/H_2O mixtures, a proportioning of 70% HFIP/30% H_2O was determined to be optimal in terms of a minimum of visible residual lyophilized protein powder or precipitate formation—higher and lower HFIP proportions both led to decreased W_3 solubilization.

Following identification of an appropriate cosolvent for spinning dope preparation, protein concentration was optimized. Wet-spinning requires a viscous solution;[9,42] however, there is a fine balance between sufficient viscosity and an overly viscous state that cannot be extruded through the spinner. Through trial and error, it was found that 5% w/v W_3 was insufficiently viscous while 10% w/v W_3 was sufficiently viscous to allow for wet-spinning, but difficult to routinely prepare and employ. Following from these observations, an optimum dope composition of 8% w/v W_3 in 70% HFIP/30% H_2O was established. The viscosities for each condition were measured (Table 1) and, corresponding to the difficulty in handling of the 10% w/v spinning dope, there is a sharp increase in the relationship between viscosity and concentration once protein concentration exceeds 8% w/v.

It should be noted that while the protein concentration in the MA gland of *Nephila clavipes* was estimated to be 50%[28] with recombinant MA-like spidroin dope production achieved at the approximate native concentration regime,[9] conditions in the anatomically distinct[26,33,60] aciniform gland have not been characterized. Significant environmental differences are also to be expected on the basis of a recent proteomics study in *N. clavipes*.[61] Specifically, disparate numbers of proteins such as ion transporters and enzymes involved in post-translational modification were identified in the MA versus aciniform glands.[33] Given the highly distinctive primary and secondary structuring of AcSp1 (vide supra), alongside the differences in behavior during wet-spinning noted herein, we have no data available to assist in emulating the natural dope conditions. The ability to produce a dope containing AcSp1 at ~8% w/v therefore cannot be directly compared to MA spidroin derived dopes nor to the native situation.

Table 1. Viscosities of W_3 Solutions in 70% HFIP/30% H_2O at Room Temperature (22.5°C)

W_3 (w/v)	viscosity (mPa·s)[a]
0	2.36 ± 0.05
5%	10.49 ± 0.20
8%	15.56 ± 0.31
10%	35.53 ± 0.71

[a]Viscosity values are averaged from triplicates; error based on microviscometer accuracy.

Secondary structuring of W_3 in the spinning dope was evaluated by far-UV CD spectroscopy (Figure 2). The high protein concentration in the dope (speaking from a CD spectroscopy standpoint) necessitated dilution to reliably characterize ellipticity below ~205 nm even at the shortest possible path length (10 μm). The diluted spinning dope exhibited a positive band at 193 nm and negative bands at 208 and 222 nm, consistent with significant α-helical content.

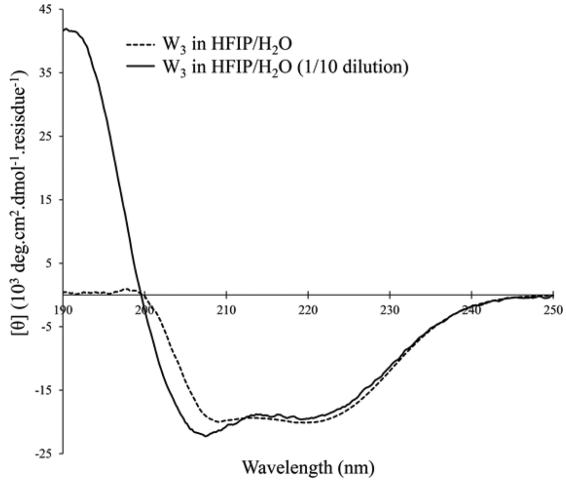

Figure 2. Far-UV CD spectra of W_3 spinning dope at ~8% w/v in 70% HFIP/30% H_2O.

The CD spectral features and mean residue ellipticities are highly similar to those we observed for W_{1-4} at much lower concentration (~0.006% w/v) in 50 mM phosphate buffer at pH 7.5.[36] These data are also consistent with our solution-state nuclear magnetic resonance (NMR) spectroscopy structure of W_1 and characterization of W_2, demonstrating that each W unit contains a globular α-helix and β-turn-rich domain connected to its neighbor(s) by intrinsically disordered linkers.[32] Notably, W_2 fibers could be hand-pulled directly from NMR samples (0.08−0.8% w/v in 20 mM sodium acetate buffer at pH 5). The

DOI: 10.1021/acs.biomac.6b00857
Biomacromolecules 2016, 17, 2737−2746

observed α-helix rich W unit structuring is consistent with polarized Raman spectromicroscopy of native AcSp1 in the gland.[34]

Two caveats should be made in this interpretation. First, fluorinated alcohols are capable of inducing helical structuring.[62,63] As such, the observed secondary structuring could be argued to be favored by the solvent environment. Conversely, it could be argued that helical stabilization by HFIP is assisting in ensuring appropriate W_3 conformation at higher concentrations than is feasible in aqueous solution. The second caveat is that CD spectroscopy itself is relatively insensitive to subtle conformational changes. As an example, a variety of W_1 Trp mutants exhibited unperturbed CD spectra despite significant perturbation to some backbone ^1H and ^{15}N chemical shifts observed by solution-state NMR.[64] However, despite these visible NMR spectral perturbations the corresponding W_2 mutants could still be hand-drawn to form fibers. As a whole, the α-helical structuring of individual W units in the dope therefore appears relatively insensitive to environment with an apparent requirement for a significant volume fraction of water to favorably solubilize the aciniform spidroin.

Wet-Spinning of W_3 Spinning Dope. A wet-spinning method to form W_3 fibers from this spinning dope in a continuous manner was next developed. To do so, we extruded the dope at a controlled rate through PEEK tubing into a coagulation bath containing a dehydrating solvent at room temperature (~22 °C). Although, as detailed above, several other recombinant spidroins have been wet-spun into fibers, wet-spinning of aciniform silk has not been previously reported. With other recombinant spidroins, either isopropyl alcohol or methanol have been used as dehydrating solvents.[9−12,14,15,42−45,58,59] Dehydration baths of 100% isopropyl alcohol and 100% methanol, alongside 100% acetone, were tested but were not efficacious for W_3 fiber production. Conversely, 95% EtOH/5% H_2O was effective, providing a cost-effective dehydrating solvent. This afforded reliable and consistent formation of fibers of sufficient mechanical integrity (termed AS fibers; Figure 3) to be handled throughout the wet-spinning process. AS W_3 fibers frequently exhibited heterogeneity in morphology and diameter by optical microscopy. To ensure that AS fiber mechanical properties could be accurately determined on the basis of a consistent diameter, fibers exhibiting extensive variation in diameter were excluded from further characterization. Following exclusion of this class of fiber, diameters at this stage were 23 ± 1 μm.

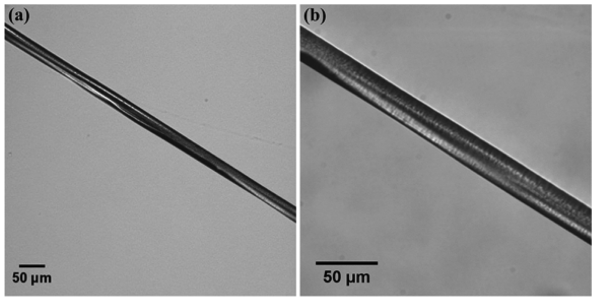

Figure 3. Light microscope images of representative AS fibers formed from wet-spinning. Images were taken at both (a) 100× magnification and (b) 400× magnification.

Post-Spin Stretching of AS W_3 Fibers. In an attempt to promote favorable structural changes that have been shown to improve mechanical properties for other silks,[9,12,43,51−53] post-spin stretching of AS W_3 fibers was carried out. Notably, organic solvent is typically employed in the post-spin stretching step because many silk-based AS fibers cannot withstand water penetration without being dissolved.[9,11,12,15,42,44,45,59] A multi-step post-spin stretching treatment is therefore often employed with the first step using an organic solvent/H_2O mixture followed by additional step(s) containing higher proportion(s) of H_2O[9,11,44,45,59] and in some cases ultimately 100% H_2O.[11,45]

Strikingly, AS W_3 fibers did not dissolve in H_2O and could therefore be directly stretched in 100% H_2O. Most studies characterizing post-spin stretching of silk-based fibers have reported carrying out this step manually with the use of forceps or tweezers,[9,11,12,42] with some reports of using controlled post-spin stretching apparatuses (for example, refs 16 and 44). An apparatus can certainly be envisioned that incorporates post-spin stretching as part of an automated fiber production process.[16,44] However, this requires knowledge of the optimal degree of post-spin stretching. To determine this optimal ratio and minimize variability introduced by hand-stretching, a post-spin stretching apparatus was built (Figure 1), which greatly increased the convenience, reliability, and consistency of this step. Post-spin stretching of AS W_3 fibers at 6× their original length was possible in H_2O without breakage for the majority (~80%) of fibers. Through optimization, it was found that stretching to 4× the original length resulted in no fiber breakage. It should also be noted that all post-spin stretching ratios discussed herein exhibited behavior consistent with plastic deformation. This provided PS fibers of highly uniform morphology and diameter (Figure 4) relative to AS W_3 fibers.

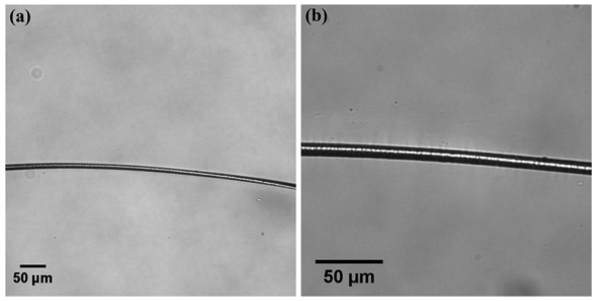

Figure 4. Light microscope images of representative PS 4× fibers formed from wet-spinning. Images were taken at both (a) 100× magnification and (b) 400× magnification.

Post-spin stretching resulted in the expected decrease in diameter relative to the AS state (Table 2) with final diameters being less than anticipated for compaction of a cylinder strictly on a volumetric basis. It should also be noted that diameters of wet-spun W_3 fibers are much greater than those observed for hand-drawn W_2 or W_4 fibers or for native wrapping silk (Table 2). On the basis of the lengths and diameters measured pre- and post-spin stretching, Poisson ratios were estimated to be ~0.48 and 0.20 for PS 2× and PS 4× fibers, respectively. In the former case, this is nearly at the upper limit of Poisson's ratio and comparable to that observed for rubber while the latter case is near the lower limit for an isotropic material.[55] The observed value of the Poisson ratio for PS 4× fibers will be further discussed later.

W_3 Fiber Mechanical Properties. Mechanical properties of AS, PS 2×, and PS 4× W_3 fibers were compared by tensile testing (representative stress−strain curves, Figure 5; resulting

DOI: 10.1021/acs.biomac.6b00857
Biomacromolecules 2016, 17, 2737−2746

Table 2. Mechanical Properties of AS, PS 2×, and PS 4× W_3 Fibers[a]

fiber type	strength (MPa)	extensibility (%)	toughness (MJ·m^{-3})	Young's modulus (GPa)	diameter (μm)	number measured
AS W_3	36 ± 12	3.1 ± 1.0	0.5 ± 0.2	1.4 ± 0.8	23 ± 1	15
PS 2× W_3	48 ± 7	2.5 ± 1.1	0.6 ± 0.2	2.5 ± 1	12 ± 1	8
PS 4× W_3	92 ± 8	2.6 ± 0.6	1.3 ± 0.3	4.5 ± 0.5	9 ± 1	12
hand-drawn W_2[32]	67 ± 16	31 ± 11	18 ± 10	1.7 ± 0.7	1.5 ± 0.1	10
hand-drawn W_3[b]	79 ± 28	21 ± 10	14 ± 8	2.8 ± 0.8	1.8 ± 0.1	7
hand-drawn W_4[36]	115 ± 24	37 ± 11	34 ± 14	2.4 ± 0.5	3.4 ± 0.3	10
AcSp1[17]	687 ± 56	86 ± 3	376 ± 39	~10 ± 4	0.35 ± 0.01	not given

[a]For context, properties are shown for hand-drawn W_2, W_3, and W_4 alongside native (~$W_{14(\text{or more})}$ + non-repetitive N- and C-terminal domains) AcSp1 from *A. trifasciata*. [b]Determined in 50 mM phosphate buffer (pH 7.5) in an identical manner to hand-drawn W_2.

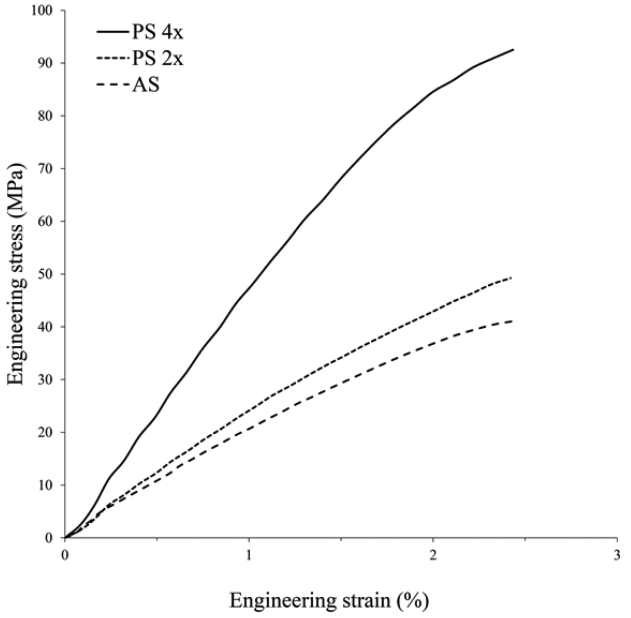

Figure 5. Representative stress−strain curves for AS, PS 2×, and PS 4× W_3 fibers (aggregate data are in Table 2).

tensile properties alongside those of hand-drawn W_2, W_3, W_4, and native AcSp1, Table 2). Extensibility was comparable in all cases at ~3%. A dramatic increase in strength and, correspondingly, toughness is apparent for PS 4× fibers relative to either AS and PS 2× fibers. An increase in Young's modulus is also apparent, increasing approximately proportionally as a function of the post-spin stretching ratio. These results are consistent with previous reports on the effects of post-spin stretching upon mechanical properties of wet-spun silk-based fibers.[9−12,15,42−45,59] Additionally, the tensile properties of these fibers fall within the range of previously reported wet-spun fibers from recombinant spidroin solubilized in HFIP. For other types of spidroin, strength and extensibility have ranged between 7 and 36 MPa and 1−5% for AS fibers,[9,11,12,42,44,59] and 14−508 MPa and 3−307% for PS (3−6×) fibers.[9−12,42−44,59] They are also consistent with reports of post-spin stretching nonsilk-based protein fibers in water, specifically native[65] and regenerated[66] hagfish slime threads as well as recombinant vimentin fibers.[67]

The observed strength of PS 4× W_3 fibers falls between those of hand-drawn W_2 and W_4, with strength tracking as a function of molecular weight. Native wrapping silk exhibits a much higher strength; however, this is coincident with a molecular weight at least 5−6× that of W_3. The current wet-spinning method notably leads to a much less extensible material than either hand-drawn recombinant AcSp1 or native wrapping silk; the observed extensibility is <10% of that of either W_2 or W_4 fibers and <4% that of native wrapping silk with correspondingly lower toughness values. The reason for the relatively low observed extensibility for wet-spun W_3 is currently not clear. In general, the decreased extensibility of wet-spun W_3 using the present conditions provides further impetus for developing an improved understanding of structure−function relationships in AcSp1. Finally, stiffness (from Young's modulus) for PS 4× W_3 fibers falls between those of hand-drawn recombinant fibers and native wrapping silk. As a whole, this provides a promising start for AcSp1 wet-spinning; identification of conditions amenable to AcSp1 that are notably disparate from other wet-spun spidroins both for spinning and post-spin stretching is critical for further modulation of mechanical properties.

Interestingly, Lin et al. demonstrated that wet-spun recombinant tubuliform spidroin 1 (TuSp1) exhibited a much lower extensibility than the native counterpart.[59] This was also accompanied by a greater tenacity for the recombinant fiber, which may be due to the relatively large size of recombinant TuSp1 protein construct (~378 kDa) that was employed. Perhaps of note, the TuSp1 repetitive domain is more similar in architecture to that of AcSp1 than the other spidroins with repeats of ~180 amino acids; however, TuSp1 is distinctive in having both a low Gly content and disparate mechanical properties.[59,68] The tertiary structure of the TuSp1 repeat unit in solution is also distinct from that of the W unit in that it is a tightly packed orthogonal 6-helix bundle.[69] As a whole, therefore, the potential generality of the low extensibility that has been observed for wet-spun recombinant AcSp1 and TuSp1 remains to be seen.

Focusing on the improved strength afforded by post-spin stretching and following precedents with both natural and recombinant MA silk,[12,15,70−72] this improvement likely results from strain-induced promotion of molecular alignment and intermolecular hydrogen-bonding within the fiber. In particular, it is likely that the AS W_3 fiber is kinetically trapped in a state where a partial crystalline phase transition has been achieved without complete oriented β-sheet microcrystal formation. Post-spin stretching is likely to provide additional extension of amorphous regions of the protein alongside increased orientation of β-sheet components, thereby promoting further stacking/aggregation into β-sheet microcrystals that are associated with increased strength of silks.[15,70] Because of the clear improvement in strength at the PS 4× stretch ratio relative to either the AS state or PS 2× stretch ratio, AS and PS 4× fiber states were comprehensively compared.

Characterization of Fibrillar Anisotropy by Birefringence. To test for increased molecular orientation following post-spin stretching, fiber birefringence was characterized using polarized light microscopy (Figure 6, insets). A notable increase

DOI: 10.1021/acs.biomac.6b00857
Biomacromolecules 2016, 17, 2737−2746

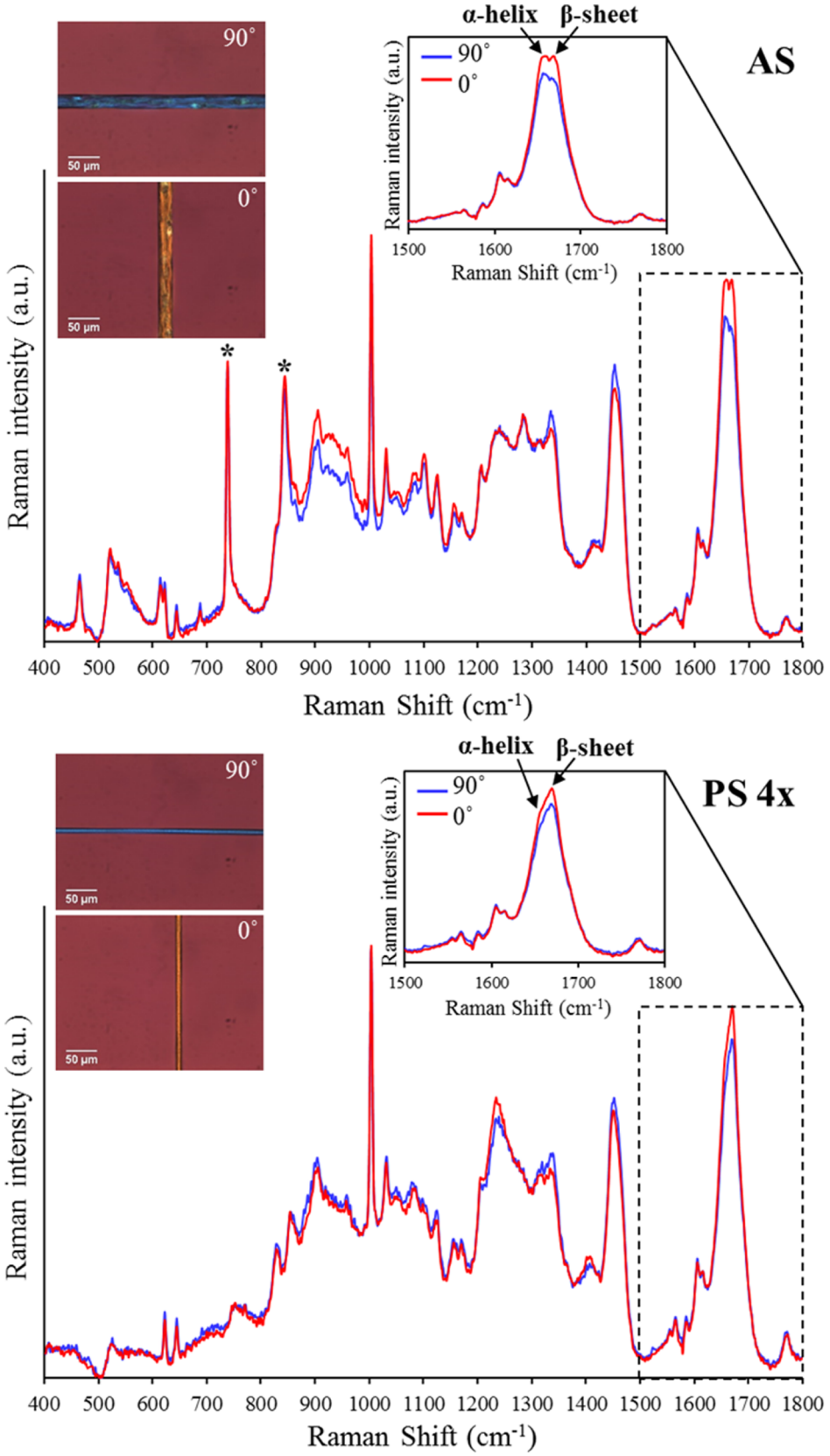

Figure 6. Raman spectra of indicated W_3 fiber with incident polarized light perpendicularly (90°) or parallel (0°) to fiber long-axis. Insets give expansions of amide I bands alongside polarized light micrographs demonstrating birefringence.

in birefringence was observed followed from post-spin stretching, suggesting an increase in alignment of protein molecules within the PS W_3 fibers. In turn, this implies increased degrees of molecular orientation and uniformity within these fibers, correlating directly to the improved mechanical strength as reported in other wet-spun silk-based

DOI: 10.1021/acs.biomac.6b00857
Biomacromolecules 2016, 17, 2737−2746

fibers.[47,73] These results agree with previous reports of post-spin stretching of wet-spun silk-based fibers, where increased birefringence correlated with improved mechanical properties such as strength.[47,73]

Fiber Secondary Structure Analysis. Having observed both an improvement in mechanical properties and an increase in birefringence following post-spin stretching of AS W_3 fibers, the potential of concomitant change in protein secondary structure was characterized using Raman spectromicroscopy. Changed secondary structuring is indeed apparent between the AS and PS 4× W_3 fiber states (Figure 6). This is particularly clear in the amide I region, where AS W_3 fibers exhibit a mix of α-helical and β-sheet conformation which becomes further enriched in β-sheet conformation in PS 4× W_3 fibers (insets in Figure 6; decompositions in Figure 7). This is consistent with both native wrapping silk structuring[32,33] and hand-drawn W_2 fibers,[32] which also exhibit a mixture of β-sheet and α-helical content.

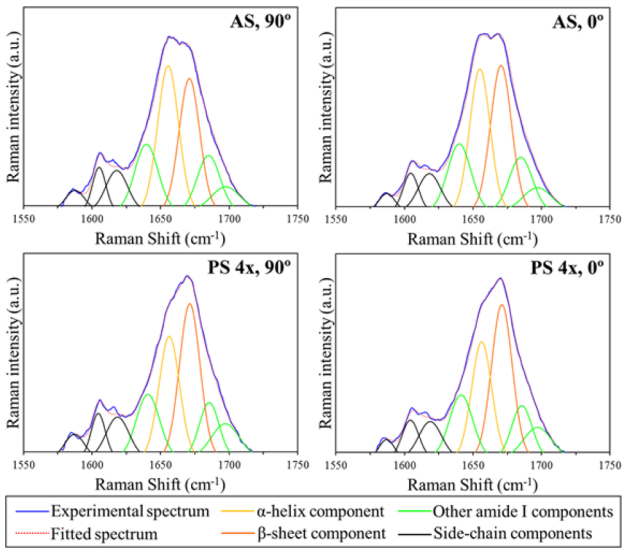

Figure 7. Decomposition of the amide I region from Raman spectra of the indicated W_3 fiber with incident light polarized perpendicularly (90°) or parallel (0°) to the fiber long-axis (corresponding to spectra in Figure 6).

Although post-spin stretching of MA silk may increase β-sheet content,[12] the general behavior of MA silk discussed above implies that post-spin stretching results in association of amorphous β-sheets to form oriented β-sheet microcrystallites. With W_3, post-spin stretching resulted in enrichment of β-sheet character and a corresponding depletion (but, corresponding to native aciniform silk, not a complete loss) of α-helical character. The differences between the polarized Raman spectra observed at orientations parallel versus perpendicular to the fiber long-axis alongside birefringence are consistent with structural anisotropy in both AS and PS 4× W_3 fibers. In short, it is difficult to unambiguously distinguish between a simple enrichment of β-sheet character versus an increase in β-sheet microcrystallites; however, at least some degree of microcrystallite enrichment is implied by the ∼2.6-fold (significant with $P < 0.001$) improved mechanical strength resulting from post-spin stretching (Table 2).

Internal and Surface Morphologies of W_3 Fibers. Fibers were immersed in liquid nitrogen and broken to allow comparison of internal morphology. SEM micrographs of fractured AS and PS 4× W_3 fiber ends (Figures 8 and 9) demonstrate that W_3 fibers are solid and tightly packed. Surface

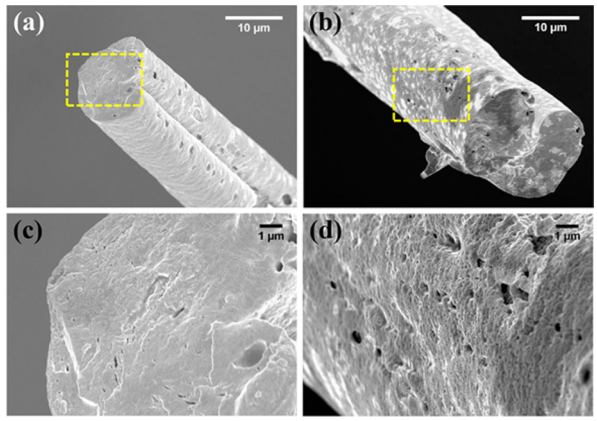

Figure 8. Representative SEM micrographs of AS W_3 fibers imaged (a–d) following fracture in liquid nitrogen.

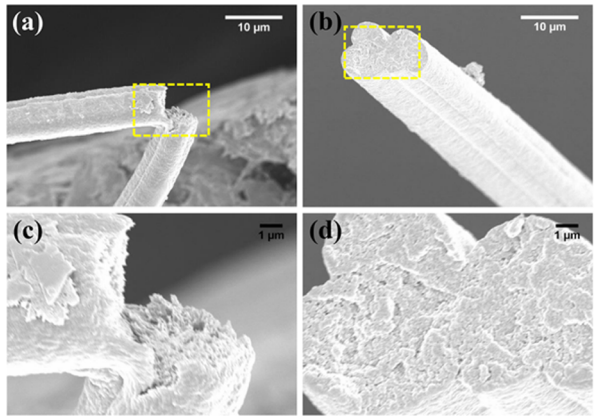

Figure 9. Representative SEM micrographs of PS 4× W_3 fibers imaged (a–d) following fracture in liquid nitrogen.

morphologies of W_3 fibers were also apparent by SEM (Figures 8 and 9). Intermittent-contact AFM allowed for a more detailed analysis of surface morphology of PS 4× fibers (Figure 10). AS fibers were not amenable to AFM as their diameters were prohibitively large relative to the height range of the scanning head. Surface striations are apparent in the surface morphology observed by SEM (e.g., very clearly in Figures 8a and 9b). By AFM, these striations appear consistently separated by ∼250 nm (arrowheads in Figure 10d). Each periodic striation exhibits features giving rise to observable roughness perpendicular to the fiber long-axis, rather than exhibiting a completely smooth topology on the size scale (∼20 nm) of the AFM tip.

A significant contrast between AS and PS 4× fiber morphology (Figures 8 and 9) is the presence of small pores (typically ∼1 μm in diameter) on the surface of AS W_3 fibers. Pores are also visible in cross sections of these fibers. These likely arise from HFIP retention in or association with the fiber following wet-spinning, consistent with distinct Raman bands at ∼739 and ∼846 cm^{-1} attributable to HFIP.[74] These bands are observed only for AS W_3 fibers (Figure 6; marked with asterisks) with that at 846 cm^{-1} obscuring two protein bands at 829 and 851 cm^{-1} most likely attributable to Tyr[33] and consistent with the presence of 12 Tyr residues per W_3 molecule. Although HFIP and H_2O are completely miscible,[75]

DOI: 10.1021/acs.biomac.6b00857
Biomacromolecules 2016, 17, 2737–2746

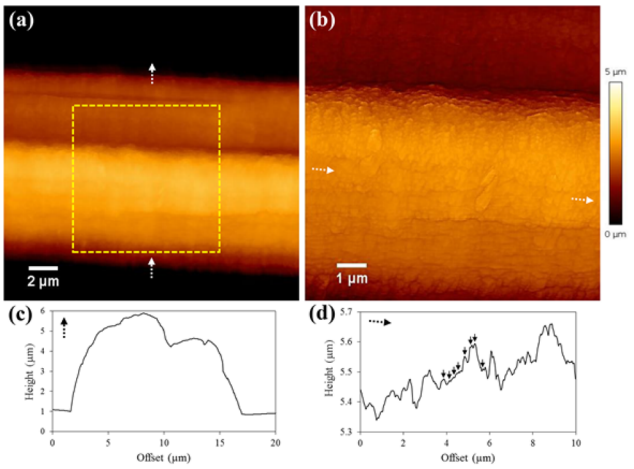

Figure 10. Representative intermittent-contact mode AFM height images of PS 4× W_3 fibers (boxed region in (a) is shown in (b); color scale is identical in (a,b)). (c) Cross-section across the fiber along arrows in (a). (d) Longitudinal section down fiber long-axis along arrows in (b). Short arrows in (d) are spaced with an ∼250 nm periodicity.

there is an HFIP mole fraction-dependent tendency to form micellar structures (radius of gyration ∼14 Å[76]) or larger alcohol-rich regions detectable by X-ray scattering.[75] In all cases, pores were absent from PS 4× W_3 fiber morphology, again consistent with the lack of corresponding HFIP-associated Raman bands. The loss of HFIP may be the result of both desorption of residual surface-associated HFIP during water immersion in post-spin stretching alongside compaction of the proteinaceous fiber core, thereby displacing any retained HFIP droplets. This also correlates well to the very low value of Poisson's ratio for the PS 4× fiber. Because lateral compression of a uniform material was assumed in calculation of ν (eq 1), any pockets of HFIP expelled during stretching would artificially decrease ν relative to that for the silk material.

CONCLUSIONS

In summary, recombinant W_3 aciniform spidroin was successfully solubilized at a sufficient concentration for wet-spinning allowing artificial production of fibers. The optimal solvent mixture for spinning dope preparation (70% HFIP/30% H_2O; ∼8% w/v W_3), the coagulation bath (95% EtOH/5% H_2O), and the post-spin stretching bath (100% H_2O) all differ from the conditions previously reported for other recombinant spidroins. Solubilization of W_3 in HFIP/H_2O produced a spinning dope with clear α-helical character, consistent with the structuring in the native AcSp1 gland and with previous high-resolution structural studies of W_2 in aqueous solution from which fibers can be formed. Following wet-spinning, the tensile strength of fibers was dramatically improved upon subjection to a post-spin stretching treatment. This is consistent with previous studies of other silks. The improved strength was directly correlated with enrichment in β-sheet character alongside increased birefringence. The improved strength therefore seems likely to be attributable to increased intermolecular hydrogen-bonding. By inference from studies on the effects of post-spin stretching upon MA silk, this likely arises from stacking and/or aggregation into microcrystalline β-sheet units within W_3 fibers. The present methodology allows for continuous wet-spinning of aciniform silk with appropriate secondary structuring and promising strength and Young's modulus. Although limited extensibility was observed, the identification of conditions that allow for continuous aciniform silk fiber spinning is a critical starting point for improved understanding and downstream application of this distinct class of silk.

AUTHOR INFORMATION

Corresponding Author

*E-mail: jan.rainey@dal.ca.

Notes

The authors declare no competing financial interest.

ACKNOWLEDGMENTS

Thanks to Drs. Thierry Lefèvre (Université Laval) and Muzaddid Sarker (Dalhousie University) for helpful discussions; Dr. David Waisman for CD spectropolarimeter access; Dr. Michael Lee and Brandon Scott for polarized light microscope access; Kevin Borgel and John Noddin for expert machining and helpful discussions; and, Patricia Scallion and Bruce Stewart for expert technical assistance. This work was supported by Discovery Grants from the Natural Sciences and Engineering Research Council of Canada (NSERC, to L.K., D.S.F., X.-Q.L., and J.K.R.); equipment and infrastructure Grants from NSERC (to L.K. and J.K.R.), the Canadian Foundation for Innovation (to L.K., J.K.R., and D.S.F.), and the Dalhousie Medical Research Foundation (to X.-Q.L. and J.K.R.); an NSERC Alexander Graham Bell Canada Graduate Scholarship (to N.W.-M.); an Ontario Early Researcher Award (to D.S.F.); and a Canadian Institutes for Health Research New Investigator Award (to J.K.R.)

REFERENCES

(1) Heim, M.; Keerl, D.; Scheibel, T. *Angew. Chem., Int. Ed.* **2009**, *48*, 3584−3596.
(2) Borkner, C. B.; Elsner, M. B.; Scheibel, T. *ACS Appl. Mater. Interfaces* **2014**, *6*, 15611−15625.
(3) Fu, C.; Shao, Z.; Fritz, V. *Chem. Commun.* **2009**, 6515−6529.
(4) Scheibel, T. *Microb. Cell Fact.* **2004**, *3*, 14.
(5) Doblhofer, E.; Heidebrecht, A.; Scheibel, T. *Appl. Microbiol. Biotechnol.* **2015**, *99*, 9361−9380.
(6) Fox, L. R. *Annu. Rev. Ecol. Syst.* **1975**, *6*, 87−106.
(7) Madsen, B.; Shao, Z. Z.; Vollrath, F. *Int. J. Biol. Macromol.* **1999**, *24*, 301−306.
(8) Rising, A.; Johansson, J. *Nat. Chem. Biol.* **2015**, *11*, 309−315.
(9) Albertson, A. E.; Teule, F.; Weber, W.; Yarger, J. L.; Lewis, R. V. *J. Mech Behav Biomed Mater.* **2014**, *29*, 225−234.
(10) Xia, X. X.; Qian, Z. G.; Ki, C. S.; Park, Y. H.; Kaplan, D. L.; Lee, S. Y. *Proc. Natl. Acad. Sci. U. S. A.* **2010**, *107*, 14059−14063.
(11) Teule, F.; Addison, B.; Cooper, A. R.; Ayon, J.; Henning, R. W.; Benmore, C. J.; Holland, G. P.; Yarger, J. L.; Lewis, R. V. *Biopolymers* **2012**, *97*, 418−431.
(12) An, B.; Hinman, M. B.; Holland, G. P.; Yarger, J. L.; Lewis, R. V. *Biomacromolecules* **2011**, *12*, 2375−2381.
(13) Tucker, C. L.; Jones, J. A.; Bringhurst, H. N.; Copeland, C. G.; Addison, J. B.; Weber, W. S.; Mou, Q.; Yarger, J. L.; Lewis, R. V. *Biomacromolecules* **2014**, *15*, 3158−3170.
(14) Arcidiacono, S.; Mello, C. M.; Butler, M.; Welsh, E.; Soares, J. W.; Allen, A.; Ziegler, D.; Laue, T.; Chase, S. *Macromolecules* **2002**, *35*, 1262−1266.
(15) Heidebrecht, A.; Eisoldt, L.; Diehl, J.; Schmidt, A.; Geffers, M.; Lang, G.; Scheibel, T. *Adv. Mater.* **2015**, *27*, 2189−2194.
(16) Copeland, C. G.; Bell, B. E.; Christensen, C. D.; Lewis, R. V. *ACS Biomater. Sci. Eng.* **2015**, *1*, 577−584.
(17) Hayashi, C. Y.; Blackledge, T. A.; Lewis, R. V. *Mol. Biol. Evol.* **2004**, *21*, 1950−1959.

DOI: 10.1021/acs.biomac.6b00857
Biomacromolecules 2016, 17, 2737−2746

(18) Xu, M.; Lewis, R. V. *Proc. Natl. Acad. Sci. U. S. A.* **1990**, *87*, 7120−7124.
(19) Hinman, M. B.; Lewis, R. V. *J. Biol. Chem.* **1992**, *267*, 19320−19324.
(20) Gaines, W. A., IV; Marcotte, W. R., Jr. *Insect Mol. Biol.* **2008**, *17*, 465−474.
(21) Blackledge, T. A.; Hayashi, C. Y. *J. Exp. Biol.* **2006**, *209*, 2452−2461.
(22) Chaw, R. C.; Zhao, Y.; Wei, J.; Ayoub, N. A.; Allen, R.; Atrushi, K.; Hayashi, C. Y. *BMC Evol. Biol.* **2014**, *14*, 31.
(23) Hedhammar, M.; Rising, A.; Grip, S.; Martinez, A. S.; Nordling, K.; Casals, C.; Stark, M.; Johansson, J. *Biochemistry* **2008**, *47*, 3407−3417.
(24) Ayoub, N. A.; Garb, J. E.; Tinghitella, R. M.; Collin, M. A.; Hayashi, C. Y. *PLoS One* **2007**, *2*, e514.
(25) Rising, A. *Acta Biomater.* **2014**, *10*, 1627−1631.
(26) Lewis, R. V. *Chem. Rev.* **2006**, *106*, 3762−3774.
(27) Hayashi, C. Y.; Shipley, N. H.; Lewis, R. V. *Int. J. Biol. Macromol.* **1999**, *24*, 271−275.
(28) Hijirida, D. H.; Do, K. G.; Michal, C.; Wong, S.; Zax, D.; Jelinski, L. W. *Biophys. J.* **1996**, *71*, 3442−3447.
(29) Simmons, A.; Ray, E.; Jelinski, L. W. *Macromolecules* **1994**, *27*, 5235−5237.
(30) Lefèvre, T.; Boudreault, S.; Cloutier, C.; Pezolet, M. *Biomacromolecules* **2008**, *9*, 2399−2407.
(31) Lefèvre, T.; Rousseau, M. E.; Pezolet, M. *Biophys. J.* **2007**, *92*, 2885−2895.
(32) Tremblay, M. L.; Xu, L.; Lefèvre, T.; Sarker, M.; Orrell, K. E.; Leclerc, J.; Meng, Q.; Pezolet, M.; Auger, M.; Liu, X. Q.; Rainey, J. K. *Sci. Rep.* **2015**, *5*, 11502.
(33) Lefèvre, T.; Boudreault, S.; Cloutier, C.; Pezolet, M. *J. Mol. Biol.* **2011**, *405*, 238−253.
(34) Rousseau, M. E.; Lefèvre, T.; Pezolet, M. *Biomacromolecules* **2009**, *10*, 2945−2953.
(35) Bratzel, G.; Buehler, M. J. *J. Mech Behav Biomed Mater.* **2012**, *7*, 30−40.
(36) Xu, L.; Rainey, J. K.; Meng, Q.; Liu, X. Q. *PLoS One* **2012**, *7*, e50227.
(37) Lang, G.; Jokisch, S.; Scheibel, T. *J. Visualized Exp.* **2013**, e50492.
(38) Stephens, J. S.; Fahnestock, S. R.; Farmer, R. S.; Kiick, K. L.; Chase, D. B.; Rabolt, J. F. *Biomacromolecules* **2005**, *6*, 1405−1413.
(39) Zhu, B.; Li, W.; Lewis, R. V.; Segre, C. U.; Wang, R. *Biomacromolecules* **2015**, *16*, 202−213.
(40) Yu, Q.; Xu, S.; Zhang, H.; Gu, L.; Xu, Y.; Ko, F. *J. Biomed. Mater. Res., Part A* **2014**, *102*, 3828−3837.
(41) Rammensee, S.; Slotta, U.; Scheibel, T.; Bausch, A. R. *Proc. Natl. Acad. Sci. U. S. A.* **2008**, *105*, 6590−6595.
(42) Adrianos, S. L.; Teule, F.; Hinman, M. B.; Jones, J. A.; Weber, W. S.; Yarger, J. L.; Lewis, R. V. *Biomacromolecules* **2013**, *14*, 1751−1760.
(43) Gnesa, E.; Hsia, Y.; Yarger, J. L.; Weber, W.; Lin-Cereghino, J.; Lin-Cereghino, G.; Tang, S.; Agari, K.; Vierra, C. *Biomacromolecules* **2012**, *13*, 304−312.
(44) Jones, J. A.; Harris, T. I.; Tucker, C. L.; Berg, K. R.; Christy, S. Y.; Day, B. A.; Gaztambide, D. A.; Needham, N. J.; Ruben, A. L.; Oliveira, P. F.; Decker, R. E.; Lewis, R. V. *Biomacromolecules* **2015**, *16*, 1418−1425.
(45) Lazaris, A.; Arcidiacono, S.; Huang, Y.; Zhou, J. F.; Duguay, F.; Chretien, N.; Welsh, E. A.; Soares, J. W.; Karatzas, C. N. *Science* **2002**, *295*, 472−476.
(46) Sutherland, T. D.; Church, J. S.; Hu, X.; Huson, M. G.; Kaplan, D. L.; Weisman, S. *PLoS One* **2011**, *6*, e16489.
(47) Wei, W.; Zhang, Y. P.; Zhao, Y. M.; Shao, H. L.; Hu, X. C. *Mater. Eng.* **2012**, *36*, 816−822.
(48) Ishizaka, H.; Watanabe, Y.; Ishida, K.; Fukumoto, O. *J. Seric Sci. Jpn.* **1989**, *58*, 87−95.
(49) Ki, C. S.; Lee, K. H.; Baek, D. H.; Hattori, M.; Um, I. C.; Ihm, D. W.; Park, Y. H. *J. Appl. Polym. Sci.* **2007**, *105*, 1605−1610.
(50) Yao, J. M.; Masuda, H.; Zhao, C. H.; Asakura, T. *Macromolecules* **2002**, *35*, 6−9.
(51) Teulé, F.; Cooper, A. R.; Furin, W. A.; Bittencourt, D.; Rech, E. L.; Brooks, A.; Lewis, R. V. *Nat. Protoc.* **2009**, *4*, 341−355.
(52) Zhang, F.; Lu, Q.; Yue, X.; Zuo, B.; Qin, M.; Li, F.; Kaplan, D. L.; Zhang, X. *Acta Biomater.* **2015**, *12*, 139−145.
(53) Shao, Z. Z.; Vollrath, F.; Yang, Y.; Thogersen, H. C. *Macromolecules* **2003**, *36*, 1157−1161.
(54) Kuipers, B. J. H.; Gruppen, H. *J. Agric. Food Chem.* **2007**, *55*, 5445−5451.
(55) Mott, P. H.; Roland, C. M. *Phys. Rev. B: Condens. Matter Mater. Phys.* **2009**, *80*, 132104.
(56) Gullekson, C.; Lucas, L.; Hewitt, K.; Kreplak, L. *Biophys. J.* **2011**, *100*, 1837−1845.
(57) Rousseau, M. E.; Beaulieu, L.; Lefèvre, T.; Paradis, J.; Asakura, T.; Pezolet, M. *Biomacromolecules* **2006**, *7*, 2512−2521.
(58) Teulé, F.; Furin, W. A.; Cooper, A. R.; Duncan, J. R.; Lewis, R. V. *J. Mater. Sci.* **2007**, *42*, 8974−8985.
(59) Lin, Z.; Deng, Q.; Liu, X. Y.; Yang, D. *Adv. Mater.* **2013**, *25*, 1216−1220.
(60) Vollrath, F.; Knight, D. P. *Nature* **2001**, *410*, 541−548.
(61) Dos Santos-Pinto, J. R.; Garcia, A. M.; Arcuri, H. A.; Esteves, F. G.; Salles, H. C.; Lubec, G.; Palma, M. S. *J. Proteome Res.* **2016**, *15*, 1179−1193.
(62) Hirota, N.; Mizuno, K.; Goto, Y. *Protein Sci.* **1997**, *6*, 416−421.
(63) Sonnichsen, F. D.; Van Eyk, J. E.; Hodges, R. S.; Sykes, B. D. *Biochemistry* **1992**, *31*, 8790−8798.
(64) Sarker, M.; Orrell, K. E.; Xu, L.; Tremblay, M. L.; Bak, J. J.; Liu, X. Q.; Rainey, J. K. *Biochemistry* **2016**, *55*, 3048−3059.
(65) Fudge, D. S.; Hillis, S.; Levy, N.; Gosline, J. M. *Bioinspiration Biomimetics* **2010**, *5*, 035002.
(66) Negishi, A.; Armstrong, C. L.; Kreplak, L.; Rheinstadter, M. C.; Lim, L. T.; Gillis, T. E.; Fudge, D. S. *Biomacromolecules* **2012**, *13*, 3475−3482.
(67) Pinto, N.; Yang, F. C.; Negishi, A.; Rheinstadter, M. C.; Gillis, T. E.; Fudge, D. S. *Biomacromolecules* **2014**, *15*, 574−581.
(68) Tian, M.; Lewis, R. V. *Appl. Phys. A: Mater. Sci. Process.* **2006**, *82*, 265−273.
(69) Lin, Z.; Huang, W.; Zhang, J.; Fan, J. S.; Yang, D. *Proc. Natl. Acad. Sci. U. S. A.* **2009**, *106*, 8906−8911.
(70) Simmons, A. H.; Michal, C. A.; Jelinski, L. W. *Science* **1996**, *271*, 84−87.
(71) Viney, C.; Huber, A. E.; Dunaway, D. L.; Kerkam, K.; Case, S. T. In *Silk Polymers*; Kaplan, D., Adams, W. W., Farmer, B., Viney, C., Eds.; - ACS Symposium Series 544; American Chemical Society: Washington, DC, 1993; pp 120−136.
(72) Riekel, C.; Madsen, B.; Knight, D.; Vollrath, F. *Biomacromolecules* **2000**, *1*, 622−626.
(73) Sun, M. J.; Zhang, Y. P.; Zhao, Y. M.; Shao, H. L.; Hu, X. C. *J. Mater. Chem.* **2012**, *22*, 18372−18379.
(74) Sanderson, J. M.; Ward, A. D. *Chem. Commun.* **2004**, 1120−1121.
(75) Kuprin, S.; Graslund, A.; Ehrenberg, A.; Koch, M. H. *Biochem. Biophys. Res. Commun.* **1995**, *217*, 1151−1156.
(76) Hong, D.-P.; Hoshino, M.; Kuboi, R.; Goto, Y. *J. Am. Chem. Soc.* **1999**, *121*, 8427−8433.

DOI: 10.1021/acs.biomac.6b00857
Biomacromolecules 2016, 17, 2737−2746